

Geochemistry, Geophysics, Geosystems

RESEARCH ARTICLE

10.1002/2016GC006393

Key Points:

- InSAR time series reveals deformation on or in the vicinity of six volcanoes
- Geophysical inverse models suggest magma chamber depths of 1–6 km

Supporting Information:

- Supporting Information S1
- Data Set S1

Correspondence to:

A. M. M. Rivera,
amorales@rsmas.miami.edu

Citation:

Morales Rivera, A. M., F. Amelung, and P. Mothes (2016), Volcano deformation survey over the Northern and Central Andes with ALOS InSAR time series, *Geochem. Geophys. Geosyst.*, 17, 2869–2883, doi:10.1002/2016GC006393.

Received 11 APR 2016

Accepted 21 JUN 2016

Accepted article online 23 JUN 2016

Published online 24 JUL 2016

Volcano deformation survey over the Northern and Central Andes with ALOS InSAR time series

Anieri M. Morales Rivera¹, Falk Amelung¹, and Patricia Mothes²

¹Rosenstiel School of Marine and Atmospheric Science, University of Miami, Miami, Florida, USA, ²Instituto Geofísico, Escuela Politécnica Nacional, Quito, Ecuador

Abstract We use ALOS-1 Interferometric Synthetic Aperture Radar data spanning the period of 2007–2011 to obtain time-dependent ground deformation data over all of the volcanoes in Colombia, Ecuador, and Peru. We detect deformation on or near the proximity of Galeras, Reventador, Tungurahua, Guagua Pichincha, Sangay, and Cerro Auquihuato volcanoes, uncovering previously undocumented deformation in the latter three. Deformation is attributed to changes in pressurization of the volcanic systems (Galeras, Tungurahua, Guagua Pichincha, and Cerro Auquihuato), subsidence associated with flow deposits (Reventador), and flank creep (Sangay). Our models suggest that the pressure sources are located at depths of ~1–6 km from the surface, indicating that the measurable deformation within our data is restricted to shallow magma chambers and hydrothermal systems.

1. Introduction

Volcanic deformation is one of the earliest signs of volcanic unrest potentially leading to eruptions [Sparks *et al.*, 2012]. However, volcanoes have shown to behave differently due to their complex nature. Some volcanoes have shown inflation prior to an eruption [e.g., Bagnardi and Amelung, 2012; Biggs *et al.*, 2009; Cervelli *et al.*, 2006; Chaussard and Amelung, 2012; Lu and Dzurisin, 2014; Poland *et al.*, 2012; Sturkell *et al.*, 2006], others inflate without erupting [e.g., Fournier *et al.*, 2010; Henderson and Pritchard, 2013; Pritchard and Simons, 2004], and others erupt without inflating [e.g., Biggs *et al.*, 2014; Lu *et al.*, 2013; Parks *et al.*, 2011; Pritchard and Simons, 2002].

Among the insights gained about volcanic deformation and unrest from local and regional Interferometric Synthetic Aperture Radar (InSAR) surveys include (1) mapping surface characteristics, structures, eruptive deposits, and the extent of deformation, (2) characteristics of the magma plumbing system (location, depth, geometry, and size), (3) volume of magma transported, (4) temporal evolution of deformation, and (5) precursory deformation leading to hazard mitigation [e.g., Chaussard and Amelung, 2012; Fournier *et al.*, 2010; Lu and Dzurisin, 2014; Pritchard and Simons, 2004]. InSAR techniques have been applied over 620 subaerial Holocene volcanoes, of which 161 have reported deformation [Biggs *et al.*, 2014].

InSAR has been previously used to study the volcanoes in the Northern and Central Andes from Colombia to Peru, with detected deformation at or near the following volcanoes during the period between 1992 and 2015: Galeras [Parks *et al.*, 2011] and Nevado del Ruiz [Lundgren *et al.*, 2015] in Colombia, Tungurahua [Biggs *et al.*, 2010; Champenois *et al.*, 2014] and Reventador [Fournier *et al.*, 2010] in Ecuador, Hualca Hualca [Pritchard and Simons, 2004], Sabancaya [Jay, 2014], and Ticsani [Holtkamp *et al.*, 2011] in Peru. In an effort to further assess the status of volcanoes in the Northern and Central Andes we conduct a systematic InSAR survey to obtain the displacement time series for volcanoes in continental Colombia, Ecuador, and Peru for the 2007–2010 period (with a few exceptions of images acquired during the end of 2006 and beginning of 2011).

2. Geological Setting and Eruptive Activity

The Northern and Central Andes from Colombia to Peru feature a total of 54 volcanoes active during the Holocene, 16 of which showed eruptive activity since the beginning of the last century [Global Volcanism Program, 2013]. Volcanism within this region results from the subduction of the Nazca plate beneath the

South American plate at rates varying from 55.5 mm/yr in the Northern Andes to 79 mm/yr in the Central Andes [Kendrick *et al.*, 2003]. The region between 3°S and 15°S in Ecuador and Peru is characterized by a lack of contemporary volcanism and heat flow attributed to the Peruvian flat-slab subduction segment [e.g., Eakin *et al.*, 2014].

Located within the Northern and Central Andes, six volcanoes (Galeras, Nevado del Huila, Reventador, Sangay, Tungurahua, and Ubinas) in Colombia, Ecuador, and Peru have had magmatic eruptions between 2006 and 2011 [Siebert and Simkin, 2002] (see Table S1 in Supporting Information). In the following we summarize the relevant activity of these volcanoes and of Guagua Pichincha and Cerro Auquihuato which did not erupt but at which we detected deformation.

Nevado del Huila (2.93°N, 76.03°W) is a 5364 m high andesitic-dacitic volcanic complex in Colombia, consisting of an elongated N-S trending glacial-capped volcanic chain [Huggel *et al.*, 2007]. Eruptions at this volcano started during February 2007 with a Volcano Explosivity Index (VEI) of 3, after centuries of eruptive quiescence [Pulgarín *et al.*, 2010]. The eruption phases between 2007 and 2012 were characterized by phreatic and radial fissure eruptions, dome extrusion, ashfalls, and lahars [Parks *et al.*, 2011].

Galeras (1.22°N, 77.36°W) is a 4276 m high andesitic stratovolcano and one of Colombia's most active volcanoes. Following about 7 years of quiescence, the most recent phase of volcanic activity began in March 2000 and resulted in explosive eruptions east of the main crater in 2002 and 2004 followed by infrequent eruptions at the summit crater during 2005–2014 with VEI of 2–3 [e.g., Parks *et al.*, 2011; Siebert and Simkin, 2002]. The earlier eruptions during the time period of our observations were characterized by lava dome growth followed by steam, gas, and ash explosions with incandescent material. During 2007–2011, Galeras had 13 explosive eruptions, of strombolian to vulcanian eruptive styles, with an estimated minimum erupted material of 13,044,033 m³ [Global Volcanism Program, 2011; INGEOMINAS, 2010].

Reventador (0.08°S, 77.66°W) is a 3562 m high andesitic stratovolcano located in northeastern Ecuador. One of its prominent features is a 4 km wide caldera open to the east that resulted from a large sector collapse around 19,000 year BP [Aguilera *et al.*, 1988] and has been subsequently filled by pyroclastic and lava flow deposits [Samaniego *et al.*, 2008]. After a 26 year quiescence, Reventador erupted in early November 2002 with a subplinian eruption (VEI of 4) followed by effusive emplacement of lava flows [Hall *et al.*, 2004; Samaniego *et al.*, 2008]. It has been intermittently erupting since then with periods of quiescence in between (e.g., no reported activity for 2006). During 2007 it had several strombolian to vulcanian eruptions, characterized by steam, gas, and ash explosions with incandescent material, and the emplacement of a lava flow. The most recent eruptive phase (continuing during the time of article submission) started in 2008 and was dominated by strombolian eruptions with emplacement of lava flows, followed by dome growth, strombolian to vulcanian explosions, and emplacement of lava and pyroclastic flows [Global Volcanism Program, 2012b; IGEPN, 2009a], essentially regrowing the portion of the summit which was lost in the 2002 eruption.

Guagua Pichincha (0.17°S, 78.60°W) is part of a volcanic complex, with a summit elevation of 4784 m and located ~11 km from Ecuador's capital, Quito. The last magmatic eruption phase occurred between 1998 and 2001 and was characterized by several months of phreatic activity followed by extrusion of nine dacitic lava domes, vulcanian eruptions, and pyroclastic flows [Garcia-Aristizabal *et al.*, 2007]. Several phreatic eruptions have been reported since then, including in 2008 and 2009 following a few days of increased precipitation [IGEPN, 2009b, 2010a], due to the presence of a shallow hydrothermal aquifer fed by meteoric water and magmatic fluids [Marini *et al.*, 1991].

Tungurahua (1.47°S, 78.44°W) is an andesitic stratovolcano with a summit elevation of 5023 m and one of Ecuador's most active volcanoes. It has been intermittently erupting since 1999, alternating between explosive periods characterized by both strombolian and vulcanian activity with the exception of subplinian activity in 2006, and relatively quiet intervals manifested by weak steam and ash emissions or total quiescence [Arellano *et al.*, 2008; Hall *et al.*, 2013; Hidalgo *et al.*, 2015]. One of its prominent features includes the scarp of a flank collapse that occurred 3000 years BP and left a large amphitheater on the western flank [Hall *et al.*, 1999], which has been subsequently filled with eruptive deposits.

Sangay (2.00°S, 78.34°W) is the southernmost active andesitic stratovolcano of Ecuador, with a summit elevation of 5286 m and with limited monitoring due to its remote location. It is considered the most active volcano in the Northern Andes because of its almost permanent explosive activity since 1628, characterized

Table 1. ALOS InSAR Data Summary^a

Track	Frame	Available Scenes	Volcanoes
<i>Colombia</i>			
147	0080	17	Cerro Bravo, Machin, Nevado del Ruiz, Nevado del Tolima, Romeral, Santa Isabel
149	0040	16	Nevado del Huila
150	0030	17	Purace
151	0020	18	Petacas, Purace, Sotara
152	0010	20	Dona Juana, Galeras, Petacas
153	0010	16	Azufral, Galeras
154	0000	18	Cerro Negro de Mayasquer, Cumbal
<i>Ecuador</i>			
107	7190	18	Soche
108	7170	18	Aliso, Sumaco
108	7180	18	Cayambe, Imbabura, Reventador
109	7170	17	Aliso, Antisana, Atacazo, Chacana, Cotopaxi
109	7180	17	Atacazo, Chacana, Cuicocha, Guagua Pichincha, Imbabura, Mojanda, Pululagua
109	7190	17	Chachimbiro, Cuicocha, Imbabura, Pululagua
110	7140	19	Sangay
110	7150	19	Cerro Altar, Chimborazo, Licto, Tungurahua
110	7170	19	Atacazo, Cotopaxi, Guagua Pichincha, Illiniza, Quilotoa
<i>Peru</i>			
101	6830	14	Nevados Casiri, Yucamane
101	6840	14	Tutupaca, Yucamane
102	6840	15	Huaynaputina, Ticsani, Tutupaca
102	6850	14	Huaynaputina, Ubinas
102	6890	20	Quimsachata
103	6850	15	Cerro Nicholson, El Misti
103	6860	15	Nevado Chachani, Sabancaya
104	6860	13	Huambo, Sabancaya
104	6870	21	Andahuaylillas-Orcopampa
105	6870	20	Coropuna
106	6870	20	Cerro Auquihuato, Sara Sara

^aALOS ascending data used for this study over volcanoes in Colombia, Ecuador, and Peru.

by strombolian activity with block and ash explosions [Monzier *et al.*, 1999]. Among its prominent features include scarps from two major sector collapses directed toward the east, where the avalanche deposits include megablocks that slid as single units [Monzier *et al.*, 1999]. Its last period of strombolian activity was between January and March 2015.

Cerro Auquihuato in Peru (15.07°S , 73.19°W) is a ~ 400 m high and unmonitored Holocene cinder cone within a Pliocene volcanic plateau with a summit elevation of 5009 m [Pecho, 1983]. No radiometric dating has been done at this volcano; therefore, the date of the last eruption is unknown but a prominent Holocene pahoehoe lava flow extends 12 km south of the volcano.

Ubinas (16.34°S , 70.90°W) is a 5672 m high andesitic to rhyolitic stratovolcano and the most active in Peru. No eruptions were reported for nearly 36 years until the 2006–2009 eruption phase, which was characterized by small phreatic, phreatomagmatic, and vulcanian eruptions, and strong fumarolic activity [Rivera *et al.*, 2014].

3. Data and Methods

We conduct an InSAR survey covering all the volcanoes in continental Colombia, Ecuador, and Peru. We use 465 ascending SAR scenes for 27 frames acquired between the end of 2006 and the beginning of 2011 by the ALOS satellite of the Japan Aerospace Exploration Agency (JAXA) (see Table 1) to generate nearly 2000 interferograms that were used for this study (see Data Set S1 in Supporting Information). We use pair-wise logic of interferograms to visually eliminate all epochs that are severely affected by phase distortions and streaks of decorrelation caused by ionospheric delays (17% of the acquisitions; see Text S1 and Figure S1 of the Supporting Information for examples).

3.1. InSAR Data Processing and Time Series Generation

We use the Modular SAR Processor software (MSP) [Werner *et al.*, 2000] to focus the raw SAR images and generate the single look complex images (SLC) that were then used to generate the interferograms with a

modified version of the ROI_PAC SAR software [Rosen *et al.*, 2004], which coregisters all interferograms to a master SLC. We remove topographic contributions using 90 m resolution digital elevation models (DEM) obtained by the NASA Shuttle Radar Topography Mission (SRTM), which were resampled to 30 m. We unwrap the interferograms using the Statistical-cost Network-flow Algorithm for Phase Unwrapping (SNA-PHU) [Chen and Zebker, 2001] and correct for unwrapping errors using a phase-closure technique based on the triangular consistency of interferograms [Fattah, 2015]. We select interferograms with perpendicular baselines of less than 2000 m and temporal baselines of less than 24 months, 34–38 months, and 46–50 months. Exceptions are made to these selection parameters, using interferograms with generally high coherence and manually removing incoherent interferograms.

We generate the time series in radar coordinates by inverting the fully connected network of interferograms for the phase history using the Small Baseline (SB) method [Berardino *et al.*, 2002]. Incoherent pixels are masked out using a temporal coherence threshold of 0.7 to reduce bias from phase unwrapping [Pepe and Lanari, 2006]. We correct for DEM errors in the time domain by removing the dependency of the displacement history to the perpendicular baseline history using the model-based approach of Fattah and Amelung [2013] (see Text S2 and Figures S2 and S3 of the Supporting Information for more details and illustrations of the correction and conditions to perform it). Fattah and Amelung [2013] demonstrated that their DEM error correction is less sensitive to their imperfect model as compared to the original SB approach, leading to more accurate results. Time series are then corrected for residual phase ramps due to tropospheric and/or ionospheric variations by estimating the linear or quadratic surface that best fits the interferometric phase. Finally, the displacement time series and averaged velocities are georeferenced.

The main source of noise in the InSAR measurements is attributed to atmospheric phase delays, but regional InSAR volcano deformation surveys are generally not suitable for atmospheric correction using empirical and predictive methods [e.g., Ebmeier *et al.*, 2013]. We use a reference pixel comparison approach to identify atmospheric delays over the volcanoes. We first compared the LOS displacement time series of an active volcano and a neighboring inactive volcano using points of similar elevation (elevation preferably within 100 m) to identify temporal patterns which represent deformation instead of stratified or localized turbulent atmospheric delay [Chaussard *et al.*, 2013] (this part of the approach was applied to all our volcanoes). Since our InSAR time series provides measurements relative to a reference point, and assuming that similar localized and regional atmospheric conditions exist within two points at proximity, we used a nondeforming pixel in proximity and at a similar elevation to the deforming region as a reference to minimize the atmospheric noise and obtain the LOS deformation (this part of the approach was applied at Reventador, Guagua Pichincha, and deformation near Cerro Auquihuato; see Text S3 and Figure S4 of the Supporting Information for more details on how we assess atmospheric delays for the Guagua Pichincha volcano example).

4. Results

Our result is an averaged 2007–2011 LOS velocity map for the volcanic areas of the northern Andes (see Figures 1 and 2 and Figures S11–S13 of the Supporting Information), which allows for the identification of actively deforming volcanoes with linear deformation trends. Positive LOS displacements (LOS decrease) represent movement toward the satellite (e.g., uplift), and negative LOS displacements (LOS increase) represent movement away from the satellite (e.g., subsidence). We examined displacement time series for all the volcanoes covered to search for nonlinear deformation, which could result in average LOS velocities of zero.

Our results reveal six volcanoes exhibiting deformation (five of which had either magmatic or phreatic eruptions during the time range of the analysis). Three of the volcanoes show LOS decrease indicating uplift (Guagua Pichincha, Tungurahua, and Cerro Auquihuato), two of them show LOS increase indicating subsidence (Galeras and Reventador), and one volcano shows both (Sangay). For each of these deformation centers, we present the results in the form of an averaged LOS velocity map and the LOS displacement time series in Figures 2 and 3 (see Figures S5–S13 in the Supporting Information for more illustrations of the LOS-averaged velocities and time series). LOS velocity profiles through the deforming volcanoes and their surroundings are given in Figure 2 and Figures S11–S13 of the Supporting Information.

At Galeras we observe a subtle LOS increase trend at the northeastern flank of the volcano for the entire time period of analysis (Figures 2a–2c), with a maximum average LOS displacement of -4.5 ± 2.8 cm. The signal is subtle but acceptable because measurements over the region of interest from two overlapping

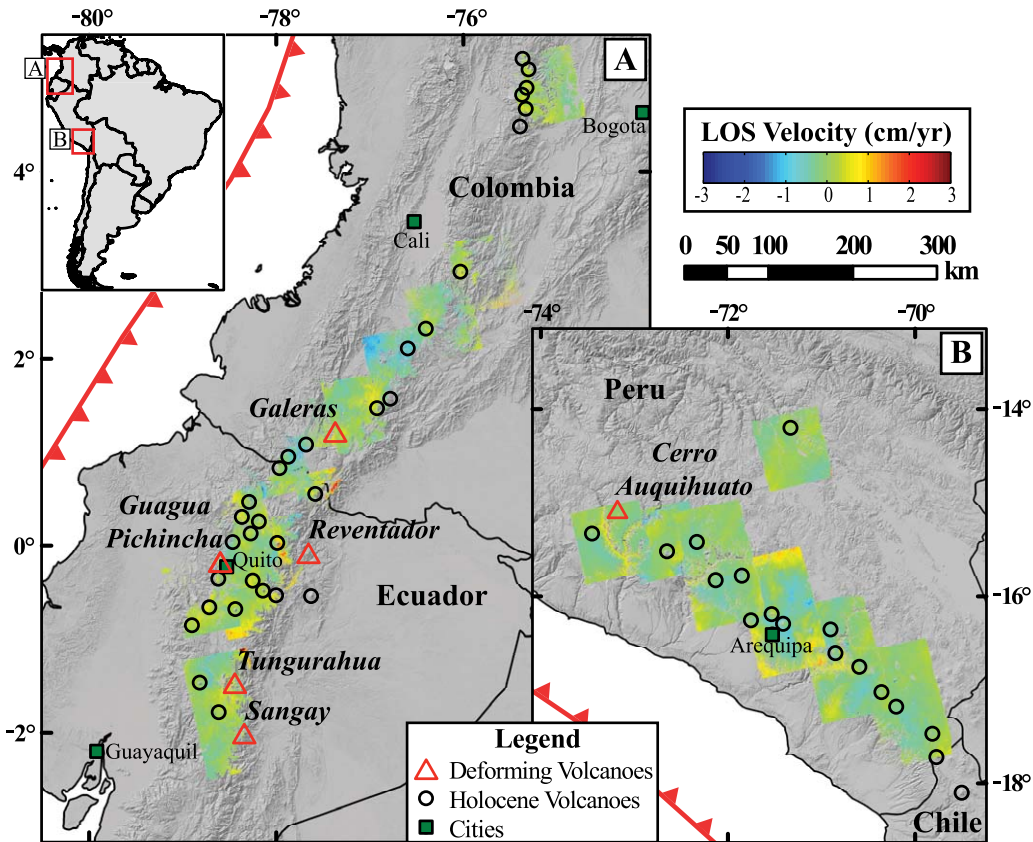


Figure 1. Averaged 2007–2011 LOS velocity map constructed with ALOS InSAR data for volcanoes under analysis in Colombia, Ecuador, and Peru (see Table 1 for ALOS track and frame information over the volcanoes). Black circles: active volcanoes during the Holocene [Siebert et al., 2010]. Red triangles: volcanoes showing deformation in this study.

satellite tracks are in agreement, as observed in Figure 2b. No evident changes can be related to individual eruption phases.

At Reventador volcano, the low interferometric coherence allows us to obtain deformation data only in the nonvegetated summit area and inside the caldera. We observe consistent LOS displacement at a rate of -6.3 ± 0.8 cm/yr centered ~ 1.5 km east of the summit for the entire observation period without evident changes related to different eruption phases. The maximum LOS displacement for the entire time period of analysis is of -22.7 ± 5 cm (Figures 3a and 3b).

At Guagua Pichincha volcano, we find previously undocumented LOS decrease on the active dome within the caldera, and immediately west and south of it, with up to 6.5 ± 1.8 cm LOS displacement from December 2006 to August 2009 (Figures 2d–2f). Figure 2e shows that measurements over the region of interest from two overlapping satellite tracks are in agreement.

For Tungurahua volcano, the average LOS velocity map shows deformation on the western flank (Figures 3c and 3d). The displacement time series for two pixels 3 km west and ~ 8 km west-southwest of the summit reveal distinct temporal behavior between the upper and lower western flank, respectively. The displacement time series for the western flank clearly reveal coeruptive LOS decrease during the period under analysis, with a noticeable increased LOS displacement rate up to 34.7 ± 1.8 cm/yr between December 2007 and May 2008 on the upper flank. Our results show that the western flank of the volcano remained inflated for the entire time period of our analysis, with a total maximum LOS displacement of 21.6 ± 1.8 cm with respect to the first date of our analysis (Figure 3c). The lack of scenes prevents us from determining if deformation clearly occurred during intereruptive periods.

Our results for Sangay volcano reveal LOS decrease on the SW flank and LOS increase on the SE flank of the volcano (Figures 2g–2i). The total maximum LOS displacements during the time range of

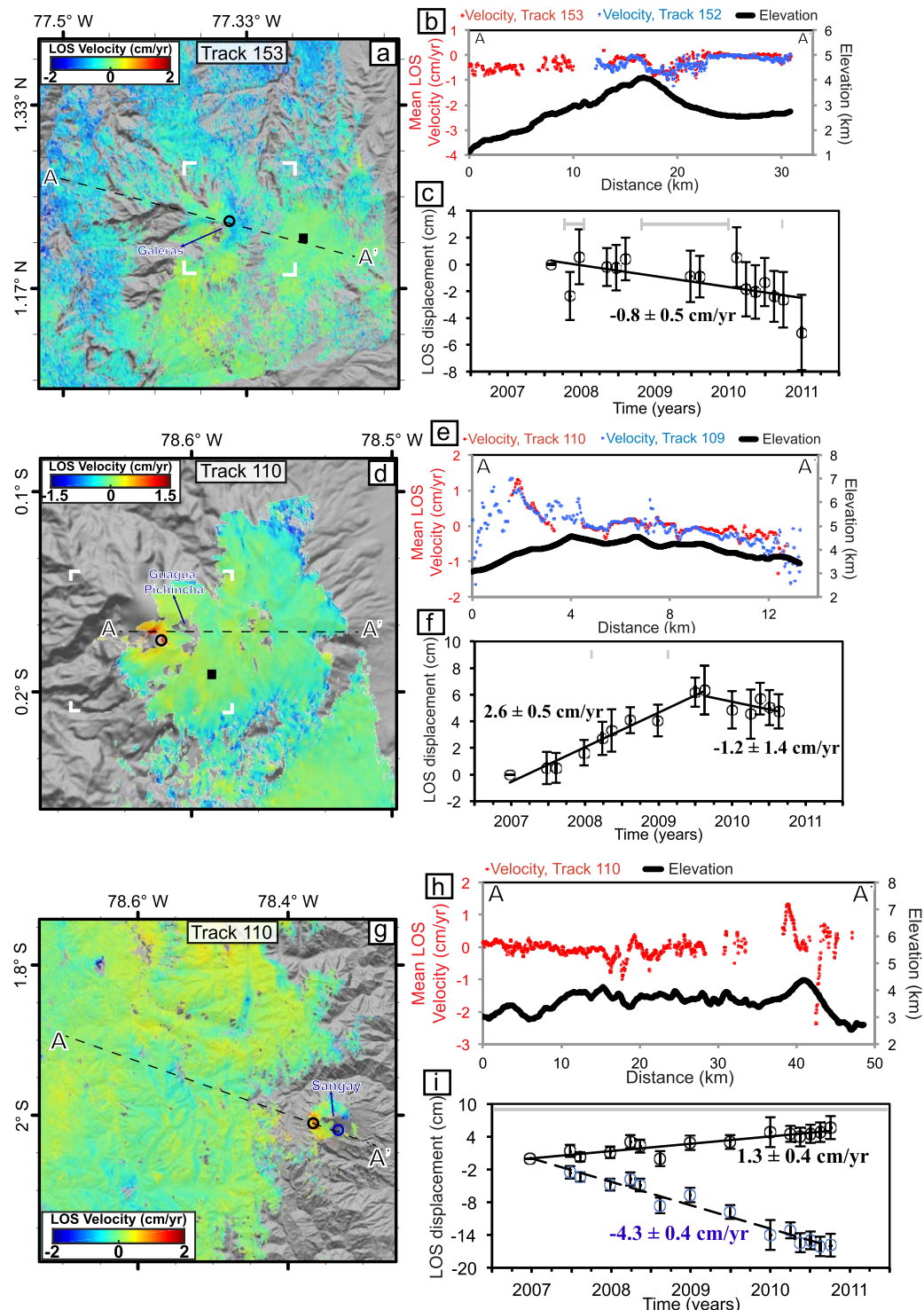


Figure 2. (left) Mean 2007–2011 LOS velocities. (top right) Mean LOS velocity profiles superimposed on the topography and (bottom right) LOS displacement time series, respectively, over (a–c) Galeras, (d–f) Guagua Pichincha, and (g–i) Sangay volcanoes. Black dashed lines in Figures 2a, 2d, and 2g: location of profiles through the deforming regions and surroundings. Reference point: solid black square in Figures 2a and 2d; $-1.4390^\circ, -78.5962^\circ$ for Figure 2g is outside the extent of the figure. White corner markers in Figures 2a and 2d: extent of Figures 4a, 4e, and 4i over Galeras, and Figures 4b, 4f, and 4j over Guagua Pichincha. Black circle in Figures 2a, 2d, and 2g: pixel for LOS displacement time series in Figures 2c, 2f, and 2i. Error bars in Figures 2c, 2f, and 2i: approximated measurement of uncertainty at each epoch, estimated using the standard deviation for all the coherent points within the frame. Gray horizontal lines in time series: periods of eruptive activity [Siebert and Simkin, 2002].

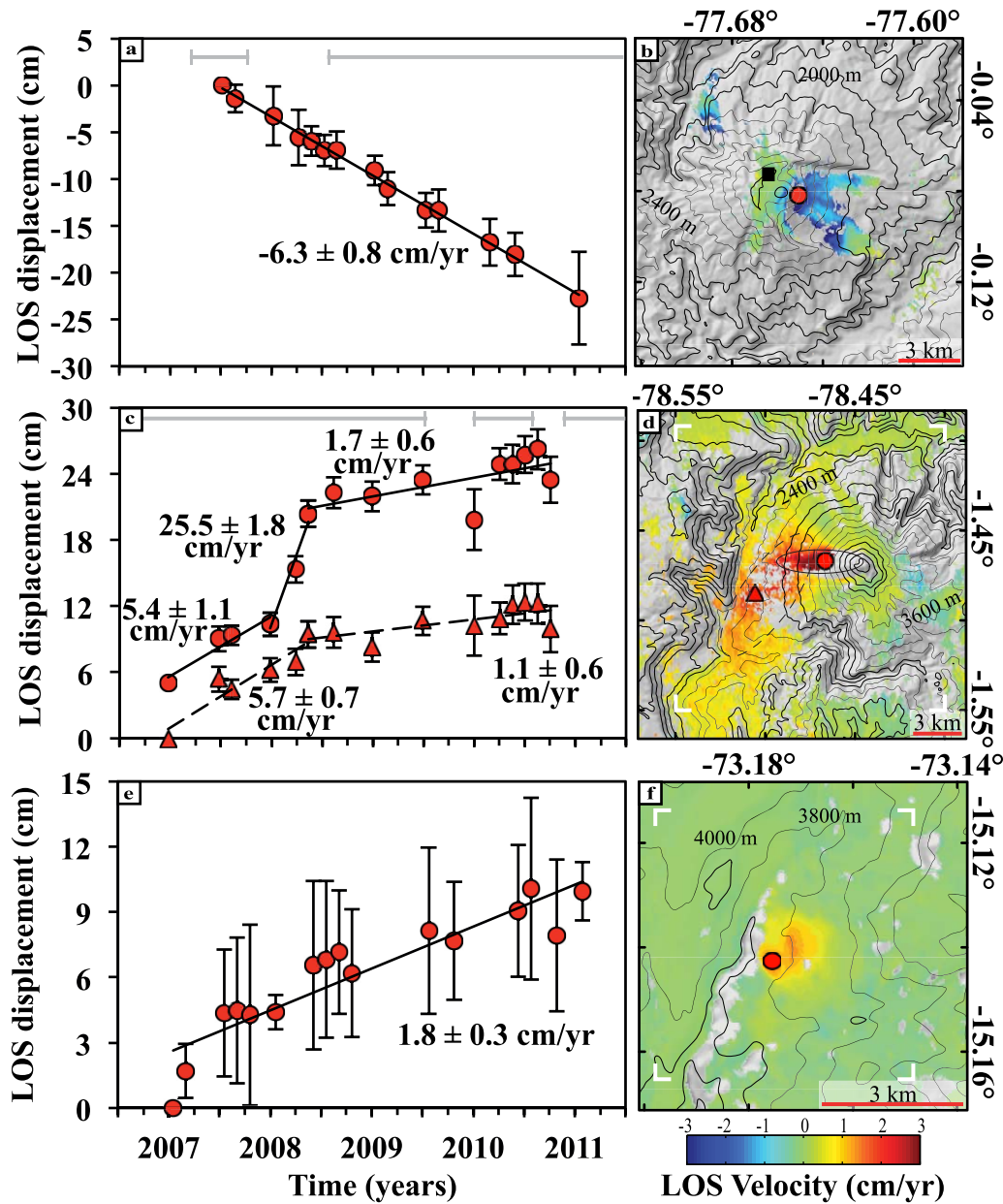


Figure 3. (left) LOS displacement time series and (right) averaged 2007–2011 LOS velocity for (a, b) Reventador, (c, d) Tungurahua, and (e, f) 7 km SE of Cerro Auquihuato volcano. For visualization purpose, the time series in Tungurahua's upper flank (circles) has been shifted upward by 5 cm. Black solid/dashed line: best-fitting linear regression for different time periods with the corresponding deformation rate. Gray horizontal lines: periods of eruptive activity [Siebert and Simkin, 2002]. Reference point: black square in Figure 3b; -1.439° , -78.5962° for Figure 3d and -15.0846° , -73.2504° for Figure 3f are outside the extents of the figures. Red circle/triangle: pixel for displacement time series. The black solid/dashed ellipsoids in Figure 3d roughly delineate two main deformation tendencies: E-W deformation trend (solid) and NE-SW trend (dashed). White corner markers in Figures 3d and 3f: extent of Figures 4c, 4g, and 4k over Tungurahua, and Figures 4d, 4h, and 4l over Cerro Auquihuato.

our study are $7.1 \pm 2.1 \text{ cm}$ and $-15.9 \pm 2.1 \text{ cm}$, respectively. Eruptions at Sangay occurred intermittently during the time period of the analysis, without evidence of surface deformation related to the eruptions.

Our results show a previously unidentified LOS decrease signal, centered at -15.1397° , -73.1714° (Figures 3e and 3f). This signal is not located in a known volcanic edifice, but is located within a valley 7 km Southeast of Cerro Auquihuato (-15.0730° , -73.1913°). The total maximum LOS displacement is $10.2 \pm 4.2 \text{ cm}$.

5. Source Modeling

We model the observed deformation using the best fitting solutions for magmatic sources embedded in a homogeneous and isotropic elastic half-space with topographic approximation [Williams and Wadge, 1998], using the University of Miami's GeodMod software. While we are neglecting the hot and mechanically heterogeneous crustal conditions along with complex source geometries and properties, these simplified models provide a first-order estimate for source depth, volume, and geometry. We use point sources [Mogi, 1958], rectangular dislocation sources with uniform opening [Okada, 1985], and pressurized ellipsoids [Yang et al., 1988]. The data are LOS displacements between two selected epochs obtained from the displacement time series, sampled using uniform grids to reduce the amount of data points (each grid dimension was nearly 90×90 m). The epochs were selected to cover the periods with linear deformation trends (the first and last epochs falling under the inflation trend for Guagua Pichincha and Cerro Auquihuato; the first and penultimate epoch covering the deflation trend for Galeras because the last epoch was noisy), and to cover nonlinear deformation during an eruption phase (e.g., nonlinear inflation at Tungurahua from 2007 until the end of the eruption phase in July 2009; see Table 2). We solve these geophysical inverse problems using a Monte-Carlo-based Gibbs sampling algorithm [Brooks and Frazer, 2005] to find the optimal solutions that yield the lowest root mean square error (RMSE).

For volcanoes showing roughly circular deformation patterns we use a Mogi model (Guagua Pichincha) or an equidimensional Okada sill model (Cerro Auquihuato). For volcanoes showing ellipsoidal patterns we use a Yang elongated spheroid model if the signal-to-noise ratio is high (Tungurahua shallow source). For volcanoes showing other elongated deformation patterns with a low signal-to-noise ratio we use rectangular Okada models (Galeras and Tungurahua deeper source). In the following we express the source depths relative to the summit elevation of each volcano, unless otherwise stated.

Our best fitting model for Galeras volcano is a volume decrease of a rectangular dislocation located at 5.9 km depth, and for Guagua Pichincha volcano a Mogi inflation source at 3 km depth (see Figure 4 and Table 2). For Tungurahua volcano two sources are required to fit the data, but these model sources have to be interpreted with caution because we have neglected the interaction between the sources [e.g., Pascal et al., 2013]. The first source is an elongated ellipsoid under the upper western flank (long axis oriented east-west) at 2.6 km depth (similar elevation as the western base of the edifice), herein referred to as the shallower source. The second source is a sill under the lower western flank (long axis oriented northeast-southwest) at 5 km depth, herein referred to as the deeper source. For the detected deformation SE of Cerro Auquihuato we find a sill at 1 km depth below the surface (surface elevation 3763 m a.s.l.; see Figure 4 and Table 2). The actual depths of the sources are probably deeper than inferred because the uppermost crust is more compliant than represented by our homogeneous models [e.g., Hautmann et al., 2010]. The model parameters and uncertainties are reported in Tables S2–S5 of the Supporting Information. We do not present models for Reventador and Sangay volcanoes because we attribute the source of deformation to other processes unrelated to magma chamber pressurization, as discussed in the following sections.

Table 2. Estimated Volcano Deformation Source Parameters

Volcano	Source	Latitude, Longitude ($^{\circ}$)	Depth ^a (km)	Length (km)	Width (km)	Opening (m)	Strike ($^{\circ}$)	Dip ($^{\circ}$)	Magnitude ^b
Galeras	Okada	12.408, -77.3236	-1.6 [-3.6]	1.8	3.8	-0.17	0	37	-1.20×10^6
Guagua Pichincha	Mogi	-0.1747, -78.6163	1.8 [-0.5]						0.12×10^6
Tungurahua	Yang (shallow source)	-1.4686, -78.4587	2.4 [0.7]	2.8	1.1		87	36	0.08×10^{-5}
	Okada (deeper source)	-1.4601, -78.4797	0.0 [-1.6]	0.3	7.7	0.79	308	-22	1.80×10^6
SE of Cerro Auquihuato	Okada	-15.1387, -73.1761	2.8 [-0.4]	1.3	1.4	0.10	199	-10	0.20×10^6

^aDepths are expressed with respect to sea level (positive and negative values are, respectively, above and below sea level), and shown in brackets with respect to the lowest topographic elevation (2028, 2346, 1678, and 3249 m for Galeras, Guagua Pichincha, Tungurahua, and Cerro Auquihuato, respectively) of the area selected around each volcano for the modeling shown in Figure 4 (positive and negative values are above and below reference elevation, respectively).

^bMagnitudes are expressed as volume change (m^3) for Okada and Mogi sources, and as pressure change (μ Pa) for Yang sources.

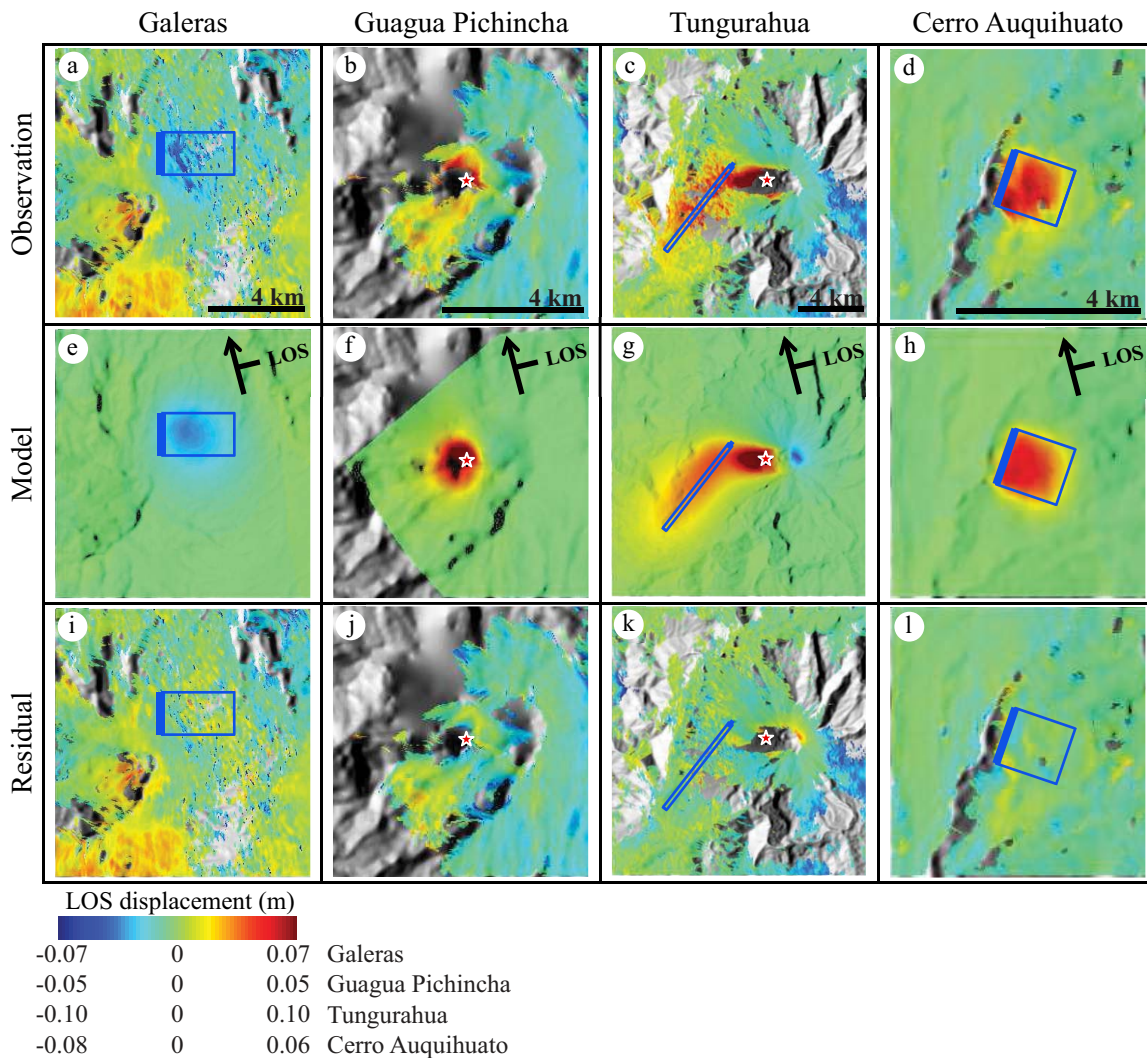


Figure 4. (a–d) Total LOS displacement maps obtained from the time series for each volcano for the periods shown in Table 2. (e–h) Predicted LOS displacements from the best-fitting models for the same periods. (i–l) Difference between the observed and the predicted LOS displacement (residuals). The blue rectangles outline the geometry of the best-fitting planar sources (sills with $<40^\circ$ inclination), the thicker line representing the shallower edge. The red star indicates the location of the best-fitting spherical/spheroidal sources (Mogi/Yang). Arrows show the flight direction of the satellite, and the black bars perpendicular to the arrows show the satellite look direction.

6. Discussion

We have identified surface deformation at/near six active volcanoes in the northern and central Andes during the 2007–2011 time period covered by ALOS InSAR. At four of the volcanoes, we have used homogeneous elastic half-space models to estimate the depth range and geometry of the sources causing the deformation. However, ground deformation can be caused by a variety of processes, including changes in pressure of the magmatic and/or hydrothermal system, subsidence of eruptive deposits and flank instability. In the following sections we compare our results with previously published studies to discuss the nature of the sources of observed deformation at/near the volcanoes.

6.1. Galeras Volcano

We have observed a LOS increase trend on the northeastern flank for the entire time period, which we have explained by long-term depressurization of a shallow magmatic source at 5.9 km depth (1.6 km b.s.l.). This is consistent with a previous study [Parks *et al.*, 2011], which identified the area of subsidence on the northeastern flank until 2008. Subsidence at volcanoes can be due to several mechanisms but several studies have presented evidence to support the presence of a shallow chamber within the northeastern flank of Galeras. Lacruz *et al.* [2009] identified seismic attenuations within the same region at 2.5 to –5 km depths

with respect to sea level, which they attributed to an area of magma accumulation. Negative Bouger and magnetic anomalies have also been identified [e.g., *Vargas and Torres*, 2015] within the same region, which can suggest, respectively, density decrease and temperatures too hot for magnetization. *Vargas and Torres* [2015] presented the velocity structure of Galeras volcano from earthquake tomography and suggested a system of ducts and fractures related to the intersection of two fault systems running through the north-eastern flank, through which magma and fluids migrate from deeper levels. Assuming the observed displacement is dominantly vertical, deformation could be explained by processes involving depressurization of a magma chamber, including drainage of magmatic or hydrothermal fluids or contraction related to cooling and crystallization of a magma chamber.

6.2. Reventador Volcano

We have observed steady LOS displacement of more than -6 cm/yr over the pyroclastic and lava flow deposits emplaced since 2002 within the sector collapse region of the volcano [e.g., *Samaniego et al.*, 2008], corresponding to more than 7.2 cm/yr of subsidence assuming that the deformation is vertical. *Fournier et al.* [2010] reported a 2008–2009 ALOS interferogram with up to -20 cm/yr LOS displacement in the southernmost collapse region. Our time series result lacks coherence over that region but we measure a maximum LOS displacement rate of -6.7 ± 2.0 cm/yr east of the summit within the collapse region (same pixel chosen for the time series shown in Figures 3a and 3b) during the same period. *Fournier et al.* [2010] attributed the deformation to cooling and compaction of pyroclastic and lava flow deposits and our results confirm these observations. Subsidence of erupted deposits has also been observed at other volcanoes [e.g., *Ebmeier et al.*, 2012; *Fournier et al.*, 2010; *Lu et al.*, 2005].

6.3. Guagua Pichincha Volcano

We have observed LOS decrease in the summit area at a fairly constant rate between 2007 and July 2009, which we have explained by a pressure source at 3 km depth (Table 2). Our source depth is much shallower than the magma storage region inferred from petrologic analysis at $\sim 5\text{--}13$ km depth below the summit [*Garcia-Aristizabal et al.*, 2007]. The observed deformation is thus caused by a shallow, previously unidentified magmatic source or it is of hydrothermal origin.

There are two arguments in favor of a magmatic origin. First, our source model depth corresponds to the base of a vertical structure identified using relocated hypocenters from volcano-tectonic earthquakes of 1998 and 1999 and interpreted as the active volcanic conduit [*Garcia-Aristizabal et al.*, 2007]. This suggests the possibility of a shallow chamber directly beneath the conduit. Second, shallow volcano-tectonic events (ranging from 0 to 7 km depth) increased during 2006 and later decreased during the second half of 2009 [IGEPN, 2010b], indicating the ascent of fluids toward the surface (e.g., from the petrologic magma body of *Garcia-Aristizabal et al.* [2007]).

However, the seismicity related to fumarolic emissions and fumarolic temperatures within the crater slightly decreased in mid-2009 [IGEPN, 2010a]. These changes coincide with the cessation of inflation in August 2009, indicating a hydrothermal origin. All this together suggests that inflation was caused by a combination of magma ascent and pressurization of the hydrothermal system, with the latter dominating. The shallow hydrothermal system was first identified by *Marini et al.* [1991].

6.4. Tungurahua Volcano

We have observed LOS decrease in the western flank of the volcano with distinct temporal and spatial characteristics, with the highest displacement rates found within the region enclosed by the rim of the flank collapse that occurred 3000 years BP [*Hall et al.*, 1999]. We attribute the source of deformation to co-eruptive inflation of two magmatic sources (see Table 2), which we roughly delineate in Figure 3d. However, we recognize that we have neglected the interaction between the two magmatic sources [*Pascal et al.*, 2013]. The shallower source with E-W orientation was initially noted by *Fournier et al.* [2010] and resembles an elongated ellipsoid, while the deeper source resembles an elongated source with a NE-SW orientation.

A previous study attributed the deformation from December 2007 to March 2008 to a single intrusion source (e.g., ellipsoidal or sill) [*Biggs et al.*, 2010]. We attempted to model the deformation with single sources (mogi, sill, and ellipsoid) but they yielded higher RMSE. Our results show a maximum LOS displacement in the western flank of the volcano of 8.4 ± 1.2 cm for this time period whereas *Biggs et al.* [2010] reported 17.5 cm of vertical displacement with negligible horizontal motion. Thus, we convert our maximum LOS into vertical displacement to obtain 10.1 cm of uplift (assuming negligible horizontal ground displacement

and an incidence angle of 34°). The differences between our results with those reported by *Biggs et al.* [2010] may arise because our methodology involves the use of time series instead of individual interferograms, as well as additional corrections to minimize errors due to residual phase ramps.

We modeled the shallower source (see Table 2) as an elongated ellipsoid, with the long axis oriented E-W. This source roughly corresponds to the base of a low-velocity zone under the northwestern flank and extends into the near-vertical structure within the edifice identified by *Molina et al.* [2005]. We modeled the deeper source (see Table 2) as a sill, with the long axis oriented NE-SW. *Molina et al.* [2005] suggested that the NNE-SSW local tectonic lineaments and faults in Tungurahua could be the preferred orientation of magma transport, which roughly agrees with the orientation of the deeper source. *Samaniego et al.* [2011] also presented petrological results for the juvenile material from the 2006 eruptions at Tungurahua and determined a magmatic source depth between 7.5 and 9.5 km below the summit. Our results show agreement with the petrological data as our models indicate that the deeper source extends into those depths.

Another study detected approximately constant large-scale inflation centered at the Tungurahua volcanic complex at a maximum LOS rate of 8.2 mm/yr near the summit using 2003–2009 Envisat InSAR time series, which they attribute mainly to a source at an intermediate depth of 16.5 km (11.5 km b.s.l.) and partly to a shallower storage zone [*Champenois et al.*, 2014]. During the ~ 2.5 year overlap with our study we do not observe clear evidence of a large-scale inflation produced by this deep source, suggesting that the deformation pattern possibly changed over time. A comparison of the results is also difficult because (1) most of their velocity estimates are less than 6 mm/yr which fall within our uncertainty estimates, (2) subtle signals produced by their deep source and measured within the edifice could be indistinguishable from those produced by shallower sources, and (3) they lose coherence on the Western flank due to decorrelation caused by eruptive deposits whereas we lose coherence directly west and south of the edifice. However, the study by *Champenois et al.* [2014] together with our results suggests an interconnected system of several magma chambers feeding the eruptions via shallow and intermediate-depth reservoirs underneath the volcanic edifice. Indeed, many of the LP seismic locations in preeruptive phases are generally at 3–5 km below the summit crater [IIGEPN, 2009c].

6.5. Sangay Volcano

For the entire time period we have detected a steady range decrease on the west flank and a steady range increase on the east flank. We attribute these signals to downhill flank motion or flank creep, although this cannot be determined using InSAR data from only one flight direction. Given the radar incidence angle of $\sim 34^\circ$ and the satellite flight azimuth of $\sim -12^\circ$, the signal along the western and eastern flanks (LOS displacement rate of up to 1.3 and -4.3 cm/yr, respectively) could be caused by ~ 3 and ~ 5 cm/yr of downhill slumping, respectively (assuming slope angles of 21 and 35° and slope azimuths of 155 and 50° , respectively). The observed deformation could also be caused by motion of the entire southern flank, where horizontal motion would go undetected in the region between the two observed signals due to motion parallel to the satellite flight direction (e.g., Arenal volcano in *Ebmeier et al.*, 2010]).

Two major sector collapses directed toward the east and southeast have been identified at Sangay [*Monzier et al.*, 1999] and the signal in the SE flank is found within these regions, which further support the hypothesis of flank creep. Flank instability at volcanoes has been previously observed elsewhere [*Ebmeier et al.*, 2010; *Schaefer et al.*, 2015; *Zhao et al.*, 2012] and poses a hazard due to the possibility of a future flank collapse, which could also be an eruption trigger.

6.6. Cerro Auquihuato

We have observed a LOS decrease trend during the entire analysis period 7 km SE of Cerro Auquihuato volcano. As the geomorphological features in the deforming area do not show any correlation with the signal, we can rule out that it is caused by local mass movements. Furthermore, the signal cannot be of anthropogenic origin because satellite optical imagery does not show roads or any other evidence for human activities in the region. The proximity to Cerro Auquihuato suggests that the signal is of volcanic origin. We attribute it to the pressurization of a magmatic source at 1 km depth below the surface (surface elevation 3763 m a.s.l.; see Table 2) but it could also be of hydrothermal origin.

7. Volcanological Implications

7.1. Lack of Deformation at Volcanoes With Magmatic Eruptions

Magmatic eruptions are expected to be associated with deformation due to changes in pressurization of the volcanic system as fluids rise toward the surface. During the time period of our observations a total of six volcanoes within our study area had reported magmatic eruptions (Nevado del Huila, Galeras, Reventador, Tungurahua, Sangay, and Ubinas), but only at one of them we observed magmatic inflation (at Tungurahua). At two volcanoes we did not observe any deformation (Nevado del Huila and Ubinas), at two volcanoes we observed subsidence of eruptive products and flank creep (Reventador and Sangay, respectively), and at one volcano we observed subsidence which we attributed to depressurization of a recurrent magma chamber (Galeras).

There are two possible volcanological reasons for the lack of detected magmatic deformation (inflation or deflation of the magma chamber) at volcanoes with magmatic eruptions. The first reason is that the volcanoes are open systems, being characterized by nearly continuous degassing and frequent eruptive activity with no significant pressurization of the system [e.g., Chaussard *et al.*, 2013; Palma *et al.*, 2008]. Of the volcanoes studied, we consider as open systems (1) Sangay volcano due to its almost permanent explosive activity since 1628 [Monzier *et al.*, 1999], (2) Galeras since 2000 and continuing into 2014 [Rose *et al.*, 2013], (3, 4) Nevado del Huila and Reventador since the 2007 eruptions, (5) Ubinas until the second half of 2009 (it had intermittent activity during 2006–2009 and again since 2013 [Masias *et al.*, 2013; OVI-INGEMMET and OVA-IGP, 2013]), and (6) Tungurahua since the beginning of the current eruption phase in October 1999.

Open plumbing systems before and during the analysis period could explain the lack of inflation at volcanoes (1)–(5). Tungurahua is an exception to this because inflation can be explained by high rates of magma supply and rapid replenishment of the magmatic system below, supported by the observation that the intruded volume of magma is larger than the erupted volume [Champenois *et al.*, 2014]. At volcanoes (1)–(6) we would expect co-eruptive deflation caused by the removal of the erupted material. However, this was not observed (with the exception of Galeras), suggesting that the magma chambers were recharged. This indicates that only minimal magma addition or gas exsolution is necessary to trigger future eruptions, which is consistent with new eruptions at these volcanoes during and after our observation period.

The second explanation for the lack of detected magmatic deformation is that the magma storage is too deep to cause detectable surface deformation. Petrological data suggest magma chamber depths of \sim 8–11 and \sim 16–19 km for Reventador and Ubinas volcanoes [Ridolfi *et al.*, 2008; Rivera *et al.*, 2014], and for Nevado del Huila volcano-tectonic earthquakes at 0–13 km depths below the summit [Global Volcanism Program, 2012a; SGC, 2014] indicate that fluids ascend from a deeper reservoir. This would be consistent with the notion that volcanic arcs in compressional stress regimes such as in the Northern and Central Andes volcanoes have few shallow reservoirs [Chaussard and Amelung, 2014].

Other possible reasons contributing to the lack of detected magmatic deformation are (1) limited temporal resolution (ALOS-1 data are available every 46 days with gaps of up to 322 days in our study; null results are possible if these systems uplift and subside with no net signal), (2) limited coverage over the area of interest due to phase decorrelation (due to Nevado del Huila's \sim 13 km 2 summit glacier and the dense vegetation in the surroundings of Reventador), (3) atmospheric disturbances over the deforming regions, and (4) limited spatial resolution could partly contribute to the decorrelation. It is also possible that signals are obscured. For example, at Reventador volcano magmatic deformation could be obscured by subsidence of the eruptive products.

7.2. Inflation Without Eruption

At or near two of the volcanoes (Guagua Pichincha and Cerro Auquihuato) we observed deformation without magmatic eruptions which can be due to many reasons, including pressurization of the chamber without reaching the failure pressure [Pinel *et al.*, 2010], rupturing of the magma chamber with conditions that prevent the magma from propagating to the surface [Gudmundsson, 2012], gas exsolution [Johnson *et al.*, 2014], and shallow hydrothermal processes [Fournier and Chardot, 2012]. All of these reasons could apply to the observed deformation at these two volcanoes, respectively.

8. Summary and Conclusions

Following our InSAR time series survey (2007–2011) over the Northern and Central Andes, we uncovered distinctive temporal deformation trends on or near three known deformation centers (Galeras, Tungurahua, and Reventador) and three not known to be deforming (Guagua Pichincha, Sangay, and Cerro Auquihuato). We attributed the observed inflation at Tungurahua volcano and deflation at Galeras volcano to changes in pressurization of the magmatic system. Deformation at Guagua Pichincha and near Cerro Auquihuato was not associated with eruptive activity but we attribute it to changes in pressurization of shallow volcanic systems. However, we cannot distinguish between a hydrothermal and magmatic origin at these two volcanoes. The location of pressure sources were estimated at depths of ~1–6 km from the surface, indicating that the measurable deformation within our time period and data is restricted to shallow magma chambers and hydrothermal systems. Deformation at Reventador volcano results from cooling and compaction of flows while we suggest that flank creep could cause the observed deformation at Sangay volcano.

Acknowledgments

The ALOS PALSAR data are copyright of the Japan Aerospace Exploration Agency (JAXA) and the Japanese Ministry of Economy, Trade, and Industry (METI). These data were made available through the Alaska Satellite Facility (ASF). We thank NASA for support through the NNX14AL39G grant. InSAR time series analysis was conducted using the PySAR software, developed at the University of Miami by Heresh Fattahi (<https://github.com/hfattahi/PySAR>). We thank C.-T. Lee, M. Pritchard, and one anonymous reviewer for their suggestions.

References

- Aguilera, E., E. Almeida, W. Balseca, F. Barberi, F. Innocenti, M. Coltellini, and G. Pasquare (1988), El Reventador: An active volcano in the sub-Andean zone of Ecuador, *Rend. Soc. Ital. Mineral. Petrol.*, 43, 853–875.
- Arellano, S. R., M. Hall, P. Samaniego, J. L. Le Pennec, A. Ruiz, I. Molina, and H. Yépes (2008), Degassing patterns of Tungurahua volcano (Ecuador) during the 1999–2006 eruptive period, inferred from remote spectroscopic measurements of SO₂ emissions, *J. Volcanol. Geotherm. Res.*, 176(1), 151–162, doi:10.1016/j.jvolgeores.2008.07.007.
- Bagnardi, M., and F. Amelung (2012), Space-geodetic evidence for multiple magma reservoirs and subvolcanic lateral intrusions at Fernandina Volcano, Galápagos Islands, *J. Geophys. Res.*, 117, B10406, doi:10.1029/2012JB009465.
- Berardino, P., G. Fornaro, R. Lanari, and E. Sansosti (2002), A new algorithm for surface deformation monitoring based on small baseline differential SAR interferograms, *IEEE Trans. Geosci. Remote Sens.*, 40(11), 2375–2383, doi:10.1109/TGRS.2002.803792.
- Biggs, J., E. Y. Anthony, and C. J. Ebinger (2009), Multiple inflation and deflation events at Kenyan volcanoes, East African Rift, *Geology*, 37(11), 979–982, doi:10.1130/g30133a.1.
- Biggs, J., P. Mothes, M. Ruiz, F. Amelung, T. H. Dixon, S. Baker, and S. H. Hong (2010), Stratovolcano growth by co-eruptive intrusion: The 2008 eruption of Tungurahua Ecuador, *Geophys. Res. Lett.*, 37, L21302, doi:10.1029/2010GL044942.
- Biggs, J., S. K. Ebmeier, W. P. Aspinall, Z. Lu, M. E. Pritchard, R. S. J. Sparks, and T. A. Mather (2014), Global link between deformation and volcanic eruption quantified by satellite imagery, *Nat. Commun.*, 5, Article 3471, doi:10.1038/ncomms4471.
- Brooks, B. A., and L. N. Frazer (2005), Importance reweighting reduces dependence on temperature in Gibbs samplers: An application to the coseismic geodetic inverse problem, *Geophys. J. Int.*, 161(1), 12–20, doi:10.1111/j.1365-246X.2005.02573.x.
- Cervelli, P. F., T. Fournier, J. Freymueller, and J. A. Power (2006), Ground deformation associated with the precursory unrest and early phases of the January 2006 eruption of Augustine Volcano, Alaska, *Geophys. Res. Lett.*, 33, L18304, doi:10.1029/2006GL027219.
- Champenois, J., V. Pinel, S. Baize, L. Audin, H. Jomard, A. Hooper, A. Alvarado, and H. Yépes (2014), Large-scale inflation of Tungurahua volcano (Ecuador) revealed by Persistent Scatterers SAR interferometry, *Geophys. Res. Lett.*, 41, 5821–5828, doi:10.1002/2014GL060956.
- Chaussard, E., and F. Amelung (2012), Precursory inflation of shallow magma reservoirs at west Sunda volcanoes detected by InSAR, *Geophys. Res. Lett.*, 39, L21311, doi:10.1029/2012GL053817.
- Chaussard, E., and F. Amelung (2014), Regional controls on magma ascent and storage in volcanic arcs, *Geochem. Geophys. Geosyst.*, 15, 1407–1418, doi:10.1002/2013GC005216.
- Chaussard, E., F. Amelung, and Y. Aoki (2013), Characterization of open and closed volcanic systems in Indonesia and Mexico using InSAR time series, *J. Geophys. Res. Solid Earth*, 118, 3957–3969, doi:10.1002/jgrb.50288.
- Chen, C. W., and H. A. Zebker (2001), Two-dimensional phase unwrapping with use of statistical models for cost functions in nonlinear optimization, *J. Opt. Soc. Am. A*, 18(2), 338–351.
- Eakin, C. M., C. Lithgow-Bertelloni, and F. M. Dávila (2014), Influence of Peruvian flat-subduction dynamics on the evolution of western Amazonia, *Earth Planet. Sci. Lett.*, 404, 250–260, doi:10.1016/j.epsl.2014.07.027.
- Ebmeier, S. K., J. Biggs, T. A. Mather, G. Wadge, and F. Amelung (2010), Steady downslope movement on the western flank of Arenal volcano, Costa Rica, *Geochem. Geophys. Geosyst.*, 11, Q1004, doi:10.1029/2010GC003263.
- Ebmeier, S. K., J. Biggs, T. A. Mather, J. R. Elliott, G. Wadge, and F. Amelung (2012), Measuring large topographic change with InSAR: Lava thicknesses, extrusion rate and subsidence rate at Santiaguito volcano, Guatemala, *Earth Planet. Sci. Lett.*, 335–336, 216–225, doi:10.1016/j.epsl.2012.04.027.
- Ebmeier, S. K., J. Biggs, T. A. Mather, and F. Amelung (2013), Applicability of InSAR to tropical volcanoes: Insights from Central America, *Geol. Soc. Spec. Publ.*, 380, 15–37, doi:10.1144/sp380.2.
- Fattahi, H. (2015), Geodetic imaging of tectonic deformation with InSAR, PhD thesis, 191 pp., Univ. of Miami, Miami, Fla.
- Fattahi, H., and F. Amelung (2013), DEM error correction in InSAR time series, *IEEE Trans. Geosci. Remote Sens.*, 51(7), 4249–4259, doi:10.1109/TGRS.2012.2227761.
- Fournier, N., and L. Chardot (2012), Understanding volcano hydrothermal unrest from geodetic observations: Insights from numerical modeling and application to White Island volcano, New Zealand, *J. Geophys. Res.*, 117, B11208, doi:10.1029/2012JB009469.
- Fournier, T. J., M. E. Pritchard, and S. N. Riddick (2010), Duration, magnitude, and frequency of subaerial volcano deformation events: New results from Latin America using InSAR and a global synthesis, *Geochem. Geophys. Geosyst.*, 11, Q01003, doi:10.1029/2009GC002558.
- García-Aristizabal, A., H. Kumagai, P. Samaniego, P. Mothes, H. Yépes, and M. Monzier (2007), Seismic, petrologic, and geodetic analyses of the 1999 dome-forming eruption of Guagua Pichincha volcano, Ecuador, *J. Volcanol. Geotherm. Res.*, 161(4), 333–351.
- Global Volcanism Program (2011), Report on Galeras (Colombia), in *Bulletin of the Global Volcanism Network*, vol. 36, edited by R. Wunderman, 5 pp., Smithsonian Inst., Washington, D. C., doi:10.5479/si.GVP.BGVN201105-351080.
- Global Volcanism Program (2012a), Report on Nevado del Huila (Colombia), in *Bulletin of the Global Volcanism Network*, vol. 37, edited by R. Wunderman, 10 pp., Smithsonian Inst., Washington, D. C., doi:10.5479/si.GVP.BGVN201210-351050.

- Global Volcanism Program (2012b), Report on Reventador (Ecuador), in *Bulletin of the Global Volcanism Network*, vol. 37, edited by R. Wunderman, 3 pp., Smithsonian Inst., Washington, D. C., doi:10.5479/si.GVP.BGVN201203-352010.
- Global Volcanism Program (2013), *Volcanoes of the World*, edited by E. Venzke, version 4.4.0, Smithsonian Inst., Washington, D.C., doi:10.5479/si.GVP.VOTW4-2013.
- Gudmundsson, A. (2012), Magma chambers: Formation, local stresses, excess pressures, and compartments, *J. Volcanol. Geotherm. Res.*, 237–238, 19–41, doi:10.1016/j.jvolgeores.2012.05.015.
- Hall, M., C. Robin, B. Beate, P. Mothes, and M. Monzier (1999), Tungurahua Volcano, Ecuador: Structure, eruptive history and hazards, *J. Volcanol. Geotherm. Res.*, 91(1), 1–21, doi:10.1016/S0377-0273(99)00047-5.
- Hall, M., P. Ramón, P. Mothes, J. L. LePennec, A. García, P. Samaniego, and H. Yépez (2004), Volcanic eruptions with little warning: The case of Volcán Reventador's surprise November 3, 2002 eruption, Ecuador, *Rev. Geol. Chile*, 31, 349–358.
- Hall, M., A. L. Steele, P. A. Mothes, and M. C. Ruiz (2013), Pyroclastic density currents (PDC) of the 16–17 August 2006 eruptions of Tungurahua volcano, Ecuador: Geophysical registry and characteristics, *J. Volcanol. Geotherm. Res.*, 265, 78–93, doi:10.1016/j.jvolgeores.2013.08.011.
- Hautmann, S., J. Gottsmann, R. S. J. Sparks, G. S. Mattioli, I. S. Sacks, and M. H. Strutt (2010), Effect of mechanical heterogeneity in arc crust on volcano deformation with application to Soufrière Hills Volcano, Montserrat, West Indies, *J. Geophys. Res.*, 115, B09203, doi:10.1029/2009JB006909.
- Henderson, S. T., and M. E. Pritchard (2013), Decadal volcanic deformation in the Central Andes Volcanic Zone revealed by InSAR time series, *Geochem. Geophys. Geosyst.*, 14, 1358–1374, doi:10.1002/ggge.20074.
- Hidalgo, S., J. Battaglia, S. Arellano, A. Steele, B. Bernard, J. Bourquin, B. Galle, S. Arrais, and F. Vásconez (2015), SO₂ degassing at Tungurahua volcano (Ecuador) between 2007 and 2013: Transition from continuous to episodic activity, *J. Volcanol. Geotherm. Res.*, 298, 1–14, doi:10.1016/j.jvolgeores.2015.03.022.
- Holtkamp, S. G., M. E. Pritchard, and R. B. Lohman (2011), Earthquake swarms in South America, *Geophys. J. Int.*, 187(1), 128–146, doi:10.1111/j.1365-246X.2011.05137.x.
- Huggel, C., J. L. Ceballos, B. Pulgarín, J. Ramírez, and J.-C. Thouret (2007), Review and reassessment of hazards owing to volcano-glacier interactions in Colombia, *Ann. Glaciol.*, 45(1), 128–136, doi:10.3189/172756407782282408.
- IGEPN (2009a), Informe de la actividad del volcán el Reventador durante el año 2008, Annual report, IGEPN, Quito, Ecuador. [Available at <http://www.igepn.edu.ec/reventador/informes-reventador/rev-anuales/647-informe-anual-reventador-2008/file>]
- IGEPN (2009b), Resumen anual de actividad 2008 volcán guagua pichincha, Annual report, IGEPN, Quito, Ecuador. [Available at <http://www.igepn.edu.ec/guagua-pichincha/informes-guagua-pichincha/ggp-anuales/11992-informe-anual-guagua-pichincha-2008/file>]
- IGEPN (2009c), Resumen de la actividad del volcán tungurahua en el 2009, Annual report, IGEPN, Quito, Ecuador. [Available at <http://158.85.9.42/tungurahua/informes-tungurahua/tung-anuales/8697-informe-anual-tungurahua-2009-1/file>]
- IGEPN (2010a), Resumen anual de actividad 2009 volcán guagua pichincha, Annual report, IGEPN, Quito, Ecuador. [Available at <http://www.igepn.edu.ec/guagua-pichincha/informes-guagua-pichincha/ggp-anuales/11993-informe-anual-guagua-pichincha-2009/file>]
- IGEPN (2010b), Resumen anual de actividad 2010 volcán guagua pichincha, Annual report, IGEPN, Quito, Ecuador. [Available at <http://www.igepn.edu.ec/guagua-pichincha/informes-guagua-pichincha/ggp-anuales/11994-informe-anual-guagua-pichincha-2010/file>]
- INGEOMINAS (2010), Boletín mensual de actividad de los volcanes del sur enero de 2010, Monthly report, INGEOMINAS, Pasto, Colombia. [Available at <http://www2.sgc.gov.co/getattachment/afffe8f5-561b-46f6-979f-eae833b79c9b/Enero-2010.aspx>]
- Jay, J. A. (2014), A geophysical survey of active volcanism in the Central and Southern Andes, PhD thesis, 279 pp., Cornell Univ., Ann Arbor, Mich.
- Johnson, J. B., J. J. Lyons, B. J. Andrews, and J. M. Lees (2014), Explosive dome eruptions modulated by periodic gas-driven inflation, *Geophys. Res. Lett.*, 41, 6689–6697, doi:10.1002/2014GL061310.
- Kendrick, E., M. Bevis, R. Smalley, B. Brooks, R. B. Vargas, E. Lauria, and L. P. S. Fortes (2003), The Nazca-South America Euler vector and its rate of change, *J. South Am. Earth Sci.*, 16(2), 125–131, doi:10.1016/S0895-9811(03)00028-2.
- Lacruz, J., A. Ugalde, C. A. Vargas, and E. Carcolé (2009), Coda-wave attenuation imaging of Galeras Volcano, Colombia, *Bull. Seismol. Soc. Am.*, 99(6), 3510–3515, doi:10.1785/0120080366.
- Lu, Z., and D. Dzurisin (2014), *InSAR Imaging of Aleutian Volcanoes: Monitoring a Volcanic Arc from Space*, 1st ed., Springer, Berlin-Heidelberg, doi:10.1007/978-3-642-00348-6.
- Lu, Z., T. Masterlark, and D. Dzurisin (2005), Interferometric synthetic aperture radar study of Okmok volcano, Alaska, 1992–2003: Magma supply dynamics and postemplacement lava flow deformation, *J. Geophys. Res.*, 110, B02403, doi:10.1029/2004JB003148.
- Lu, Z., D. Dzurisin, C. Wicks, J. Power, O. Kwoun, and R. Rykhus (2013), Diverse deformation patterns of Aleutian volcanoes from Satellite Interferometric Synthetic Aperture Radar (InSAR), in *Volcanism and Subduction: The Kamchatka Region*, edited by J. Eichelberger et al., pp. 249–261, AGU, Washington, D. C., doi:10.1029/172GM18.
- Lundgren, P., S. V. Samsonov, C. M. López Velez, and M. Ordoñez (2015), Deep source model for Nevado del Ruiz Volcano, Colombia, constrained by interferometric synthetic aperture radar observations, *Geophys. Res. Lett.*, 42, 4816–4823, doi:10.1002/2015GL063858.
- Marini, L., A. Agostini, R. Cioni, M. Guidi, and O. Leon (1991), Guagua pichincha volcano, Ecuador: Fluid geochemistry in volcanic surveillance, *J. Volcanol. Geotherm. Res.*, 46(1–2), 21–35, doi:10.1016/0377-0273(91)90073-9.
- Masias, P., E. Taipe, Y. Antayhua, and D. Ramos (2013), Monitoreo de los volcanes Misti y Ubinas, Periodo 2006–2012, 54, 104 pp., INGEMMET Lima, Peru.
- Mogi, K. (1958), Relations between the eruptions of various volcanoes and the deformations of the ground surfaces around them, *Bull. Earthquake Res. Inst. Univ. Tokyo*, 36, 99–134.
- Molina, I., H. Kumagai, J.-L. Le Pennec, and M. Hall (2005), Three-dimensional P-wave velocity structure of Tungurahua Volcano, Ecuador, *J. Volcanol. Geotherm. Res.*, 147(1–2), 144–156, doi:10.1016/j.jvolgeores.2005.03.011.
- Monzier, M., C. Robin, P. Samaniego, M. L. Hall, J. Cotten, P. Mothes, and N. Arnaud (1999), Sangay volcano, Ecuador: Structural development, present activity and petrology, *J. Volcanol. Geotherm. Res.*, 90(1–2), 49–79, doi:10.1016/S0377-0273(99)00021-9.
- Okada, Y. (1985), Surface deformation due to shear and tensile faults in a half-space, *Bull. Seismol. Soc. Am.*, 75(4), 1135–1154.
- OVI-INGEMMET and OVA-IGP (2013), Actividad reciente del volcán ubinas (1 al 3 de Septiembre 2013), 1, OVI-INGEMMET, Arequipa, Peru.
- Palma, J. L., E. S. Calder, D. Basualto, S. Blake, and D. A. Rothery (2008), Correlations between SO₂ flux, seismicity, and outgassing activity at the open vent of Villarrica volcano, Chile, *J. Geophys. Res.*, 113, B10201, doi:10.1029/2008JB005577.
- Parks, M. M., J. Biggs, T. A. Mather, D. M. Pyle, F. Amelung, M. L. Monsalve, and L. N. Medina (2011), Co-eruptive subsidence at Galeras identified during an InSAR survey of Colombian volcanoes (2006–2009), *J. Volcanol. Geotherm. Res.*, 202(3–4), 228–240, doi:10.1016/j.jvolgeores.2011.02.007.
- Pascal, K., J. Neuberg, and E. Rivalta (2013), On precisely modelling surface deformation due to interacting magma chambers and dykes, *Geophys. J. Int.*, 196, 253–278, doi:10.1093/gji/ggt343.
- Pecho, V. (1983), Geología de los Cuadrángulos de Pausa y Caraveli, in *INGEMMET Bulletin, Series A*, vol. 37, 126 pp., INGEMMET, Lima, Peru.

- Pepe, A., and R. Lanari (2006), On the extension of the minimum cost flow algorithm for phase unwrapping of multitemporal differential SAR interferograms, *IEEE Trans. Geosci. Remote Sens.*, 44(9), 2374–2383, doi:10.1109/TGRS.2006.873207.
- Pinel, V., C. Jaupart, and F. Albino (2010), On the relationship between cycles of eruptive activity and growth of a volcanic edifice, *J. Volcanol. Geotherm. Res.*, 194(4), 150–164, doi:10.1016/j.volgeores.2010.05.006.
- Poland, M. P., A. Miklius, A. Jeff Sutton, and C. R. Thornber (2012), A mantle-driven surge in magma supply to Kilauea Volcano during 2003–2007, *Nat. Geosci.*, 5(4), 295–300, doi:10.1038/ngeo1426.
- Pritchard, M. E., and M. Simons (2002), A satellite geodetic survey of large-scale deformation of volcanic centres in the central Andes, *Nature*, 418(6894), 167–171.
- Pritchard, M. E., and M. Simons (2004), An InSAR-based survey of volcanic deformation in the central Andes, *Geochem. Geophys. Geosyst.*, 5, Q02002, doi:10.1029/2003GC000610.
- Pulgarín, B., C. Cardona, C. Santacoloma, A. Agudelo, M. Calvache, and M. Monsalve (2010), Erupciones del volcán Nevado del Huila (Colombia) en febrero y abril de 2007 y cambios en su masa glaciar, in *Glaciares, Nieves y Hielos de América Latina: Cambio Climático y Amenazas Glaciares*, edited by C. D. Lopez and J. Ramirez, pp. 279–305, INGEOMINAS, Bogota, Colombia.
- Ridolfi, F., M. Puerini, A. Renzulli, M. Menna, and T. Toulkeridis (2008), The magmatic feeding system of El Reventador volcano (sub-Andean zone, Ecuador) constrained by texture, mineralogy and thermobarometry of the 2002 erupted products, *J. Volcanol. Geotherm. Res.*, 176(1), 94–106, doi:10.1016/j.volgeores.2008.03.003.
- Rivera, M., J.-C. Thouret, P. Samaniego, and J.-L. Le Pennec (2014), The 2006–2009 activity of the Ubinas volcano (Peru): Petrology of the 2006 eruptive products and insights into genesis of andesite magmas, magma recharge and plumbing system, *J. Volcanol. Geotherm. Res.*, 270, 122–141, doi:10.1016/j.volgeores.2013.11.010.
- Rose, W. I., J. L. Palma, H. Delgado Granados, and N. Varley (2013), Open-vent volcanism and related hazards: Overview, *Geol. Soc. Am. Spec. Pap.*, 498, vii–xiii, doi:10.1130/2013.2498(00).
- Rosen, P. A., S. Hensley, G. Peltzer, and M. Simons (2004), Updated repeat orbit interferometry package released, *Eos Trans. AGU*, 85(5), 47–47, doi:10.1029/2004EO050004.
- Samaniego, P., J.-P. Eissen, J.-L. Le Pennec, C. Robin, M. Hall, P. Mothes, D. Chavrit, and J. Cotten (2008), Pre-eruptive physical conditions of El Reventador volcano (Ecuador) inferred from the petrology of the 2002 and 2004–05 eruptions, *J. Volcanol. Geotherm. Res.*, 176(1), 82–93, doi:10.1016/j.volgeores.2008.03.004.
- Samaniego, P., J.-L. Le Pennec, C. Robin, and S. Hidalgo (2011), Petrological analysis of the pre-eruptive magmatic process prior to the 2006 explosive eruptions at Tungurahua volcano (Ecuador), *J. Volcanol. Geotherm. Res.*, 199(1–2), 69–84.
- Schaefer, L. N., Z. Lu, and T. Oommen (2015), Dramatic volcanic instability revealed by InSAR, *Geology*, 43(8), 743–746, doi:10.1130/g36678.1.
- SGC (2014), Informe tecnico de actividad de los volcanes Nevado del Huila, Purace y Sotara durante el Año 2013, Annual report, SGC, Popayán, Colombia. [Available at <http://www2.sgc.gov.co/getattachment/097a6bb2-b793-4a4d-88b2-f9535f14a8e0/Informe-anual-de-actividad-2013.aspx>]
- Siebert, L., and T. Simkin (2002), Volcanoes of the world: An illustrated catalog of Holocene volcanoes and their eruptions, in *Global Volcanism Program Digital Information Series GVP-3*, Smithsonian Inst., Washington, D. C.
- Siebert, L., T. Simkin, and P. Kimberly (2010), *Volcanoes of the World*, 3rd ed., 568 pp., Univ. of Calif. Press, Berkeley.
- Sparks, R. S. J., J. Biggs, and J. W. Neuberg (2012), Monitoring volcanoes, *Science*, 335(6074), 1310–1311, doi:10.1126/science.1219485.
- Sturkell, E., P. Einarsson, F. Sigmundsson, H. Geirsson, H. Ólafsson, R. Pedersen, E. de Zeeuw-van Dalfsen, A. T. Linde, S. I. Sacks, and R. Stefánsson (2006), Volcano geodesy and magma dynamics in Iceland, *J. Volcanol. Geotherm. Res.*, 150(1–3), 14–34, doi:10.1016/j.volgeores.2005.07.010.
- Vargas, C. A., and R. Torres (2015), Three-dimensional velocity structure of the Galeras volcano (Colombia) from passive local earthquake tomography, *J. Volcanol. Geotherm. Res.*, 301, 148–158, doi:10.1016/j.volgeores.2015.05.007.
- Werner, C., U. Wegmüller, T. Strozzi, and A. Wiesmann (2000), Gamma SAR and interferometric processing software, paper presented at Proceedings of the ERS-ENVISAT Symposium, European Space Agency, Gothenburg, Sweden.
- Williams, C. A., and G. Wadge (1998), The effects of topography on magma chamber deformation models: Application to Mt. Etna and radar interferometry, *Geophys. Res. Lett.*, 25(10), 1549–1552, doi:10.1029/98GL01136.
- Yang, X.-M., P. M. Davis, and J. H. Dieterich (1988), Deformation from inflation of a dipping finite prolate spheroid in an elastic half-space as a model for volcanic stressing, *J. Geophys. Res.*, 93(B5), 4249–4257, doi:10.1029/JB093B05p04249.
- Zhao, C., Z. Lu, Q. Zhang, and J. de la Fuente (2012), Large-area landslide detection and monitoring with ALOS/PALSAR imagery data over Northern California and Southern Oregon, USA, *Remote Sens. Environ.*, 124, 348–359, doi:10.1016/j.rse.2012.05.025.